Golden RAtio Stack of Spirals for flexible angiographic imaging: proof of concept in congenital heart disease

Grzegorz Tomasz Kowalik PhD[1], Jennifer Anne Steeden PhD[1], David Atkinson PhD[2], Javier Montalt-Tordera MSc[1], Kristian Mortenson MD PhD[3], Vivek Muthurangu MD(res)[1,3]

[1]UCL Institute of Cardiovascular Science, Centre for Cardiovascular Imaging, 30 Guildford Street, London, UK WC1N 1EH
[2]University College London, Centre for Medical Imaging, Wolfson House, 4 Stephenson Way, London, UK NW1 2HE
[3]Great Ormond Street Hospital for Children, Great Ormond Street, London, WC1N 3JH, UK

Corresponding author:

Dr. Grzegorz Tomasz Kowalik, Ph. D.

Centre for Cardiovascular Imaging, UCL Institute of Cardiovascular Science

Great Ormond Street Hospital for Children

Great Ormond Street, London, WC1N 3JH, UK

Tel: +44 (0)207 405 9200 ext 6834

email: grzegorz.kowalik.09@ucl.ac.uk

Running title:

Golden RAtio Stack of Spirals 3D MRA

Word count: 4208

ABSTRACT

Purpose: In this study, a Golden Ratio Stack of Spiral (GRASS) sequence that used both golden step and golden angle ordering was implemented. The aim was to demonstrate that GRASS acquisitions could be flexibly reconstructed as both cardiac gated and time resolved angiograms.

Methods: Image quality of time resolved and cardiac gated reconstructions of the GRASS sequence were compared to three conventional stack of spirals (SoS) acquisitions in an in-silico model. In ten patients, the GRASS sequence was compared to conventional breath hold angiography (BH-MRA) in terms of image quality and for vessel measurement. Vessel measurements were also compared to cine images.

Results: In the cardiac gated in-silico model, the image quality of GRASS was superior to regular and golden-angle with regular step SoS approaches. In the time resolved model, GRASS image quality was comparable to the golden-angle with regular step technique and superior to regular SoS acquisitions. In patients, there was no difference in qualitative image scores between GRASS and BH-MRA, but signal to noise ratio was lower. There was good agreement in vessel measurements between the GRASS reconstructions and conventional MR techniques (BH-MRA: 29.8±5.6 mm, time resolved GRASS-MRA: 29.9±5.4 mm, SSFP diastolic: 29.4±5.8 mm, cardiac gated GRASS-MRA diastolic: 29.5±5.5 mm, $P > 0.87$)

Conclusion: We have demonstrated that the GRASS acquisition enables flexible reconstruction of the same raw data as both time resolved and cardiac gated volumes. This may enable better interrogation of anatomy in congenital heart disease.

INTRODUCTION

Contrast enhanced MR angiography (MRA) is heavily used in the assessment of the intra-thoracic vessels (1-5), particularly in congenital heart disease. Conventionally, MRA's are acquired in a 10-25 second breath hold without cardiac gating. However, several modifications have been implemented to expand the utility of this technique.

For example, by accelerating data acquisition it is possible to image multiple volumes during the passage of contrast through the heart and vessels (6). Such time-resolved MRA techniques provide dynamic information that is not available using routine MRA. In addition, many time resolved sequences can be acquired during free breathing, making them useful when assessing children or adults with respiratory difficulty. Another recent development is cardiac gated MRA, which can be used to more accurately evaluate vessels that move or expand during the cardiac cycle (i.e. the proximal aorta) (7). One problem with cardiac gated MRA is increased acquisition time and consequently longer breath holds.

Usually only one type of MRA is performed per scan due to differing acquisition strategies. However, the ability to perform both time resolved and cardiac gated reconstructions of the same raw data would be clinically useful. This requires a sampling scheme that provides acceptable image quality irrespective of the readouts used for reconstruction.

One solution is golden ratio ordering (8,9), as it ensures optimal filling of k-space with arbitrary subsets of readouts. A further benefit of golden ratio readout ordering, is incoherent undersampling artefacts that are well suited to compressed sensing reconstruction (10,11). Golden ratio ordering has been implemented in three dimensions using a variety of acquisition strategies. These include: golden angle radial stack of stars with regular Cartesian slice encoding (10), golden angle radial Koosh-ball (12) and Cartesian with pseudo-spiral golden angle phase encoding (13). In this study, we chose to combine golden ratio ordering with a stack of spirals (SoS) approach. SoS is a proven method of rapidly acquiring volumetric data (14,15) and has been used for time resolved MRA in congenital heart disease (6). It has previously been shown that combining golden angle rotations in k_x-k_y with regular steps k_z improves sparse parallel reconstruction for both radial and spiral stacked acquisitions (10,16). However, golden ratio ordering can be further exploited by also using a golden step in k_z. The benefit of this Golden RAtio Stack of Spirals (GRASS)

approach should be greater flexibility in terms of reconstructing both time resolved and cardiac gated data.

The aims of this work were: i) to compare the image quality of both time resolved and cardiac gated reconstructions of GRASS data with more conventional SoS strategies in an in-silico model, ii) to demonstrate the feasibility of acquiring GRASS MRA data and reconstructing both time resolved and cardiac gated reconstructions in patients with congenital heart disease, and iii) to compare vessel measurements and image quality of GRASS MRA to more conventional techniques.

METHODS

This work is divided into two parts: i) an in-silico study that compares the GRASS technique to more conventional SoS approaches in a digital phantom, and ii) a patient study that compares the GRASS technique to conventional angiographic techniques. All imaging was performed on a 1.5 Tesla MR scanner (Avanto, Siemens Medical Solutions, Erlangen, Germany) using two spine coils and one body-matrix coil (giving a total of 12 coil elements).

GRASS acquisition

The GRASS sequence was based on a modified 3D spoiled gradient echo stack of spirals, with 18 uniform density regularly spaced spiral interleaves in k_x-k_y per k_z partition, and 88 regular spaced k_z partitions (fully sampled). The spiral trajectories were calculated using the method described by Hargreaves [17].

The modifications required to incorporate golden ratio ordering were based on a nested loop strategy (see supporting materials for full diagram - Supporting Fig. 1). In the inner-loop, consecutive spiral interleaves were advanced by the golden step in the k_z direction, whilst keeping their k_x-k_y position the same. The golden step equalled ~1.618 x k_z dimension, with cycling from the bottom as required. Each inner-loop consisted of 44 steps (~2x undersampling in k_z) and was followed by an outer-loop operation. The outer-loop involved rotation of the spiral interleave position in k_x-k_y by the golden angle (~222°). Scan parameters were as follows (FOV: 450x450x202 mm, Matrix: 192x192x88, pixel size: 2.3x2.3x2.3 mm, TR/TE: 9.02/1.6 ms, Flip Angle: 15°).

In patients, the intravenous contrast protocol was 0.2 mL/kg of Gadoteric acid (Dotarem, Guerbet, Roissy, France) up to a maximum of 10 mL injected at a speed of 2 mL/s. The GRASS acquisition was started at the same time as the contrast injection and data were continuously acquired for ~120 s (13332 read-outs). This time was chosen to enable collection of enough data to perform a cardiac gated reconstruction with 24 phases, 12x acceleration and respiratory navigation acceptance of 30%. After the imaging portion of the sequence, two fully sampled, regularly spaced SoS were acquired (18 spiral interleaves and 88 k_z positions, ~29 s). These were averaged to generate high signal to noise ratio coil sensitivity maps. In total, the acquisition lasted ~149 s.

GRASS-MRA reconstruction

The GRASS data were reconstructed as both time resolved and cardiac gated series in both the phantom and patient studies.

For the time resolved reconstruction, temporally non-overlapping volumes were reconstructed using 132 consecutive interleaves. This resulted in an acquisition time per volume of ~1.2 s and a total acceleration factor of twelve (~6x in k_x-k_y and ~2x in k_z).

The cardiac gated reconstruction combined data from the whole acquisition and therefore needed respiratory navigation. This was implemented using a self-gating signal that was generated by Fourier transforming points distributed along k_z at k_x-k_y = (0, 0) (Full details are described in supporting materials - Supporting Fig. 2). This signal was used to extract 30% of data associated with the most expiratory positions. The use of 30% of the data was based on a previous respiratory self-gated 2D golden angle spiral sequence that demonstrated improved image quality at this level acceptance (9). This 'expiratory' data was then binned into 24 cardiac phases depending on their linearly-normalized position in an average r-r interval (18). The result was retrospectively cardiac gated volume data across the whole cardiac cycle.

All GRASS data was reconstructed offline using a non-linear Conjugate Gradient algorithm that was implemented on an external GPU equipped computer (Tesla K40c, NVIDIA, Santa Clara, CA, USA). The CS reconstruction used a finite difference operator applied in the temporal domain. This operation applied to data with relatively small number of frame-to-frame changes can transform it into a sparser representation. This was similar to the previously described golden-angle radial and spiral sparse parallel reconstructions (10,19). For the in-silico study, multiple CS reconstructions with different regularizations were performed for each sampling pattern. In the patient study, the regularisation level was selected empirically on a single patient to minimize artefact without producing obvious visual temporal blurring and used for all subsequent patient data.

In-Silico study

An in-silico model was used to assess the performance of the GRASS acquisition compared to three conventional SoS approaches: i) fully regular SoS (REG) -

consecutive read-outs were advanced by a regular step in the k_z direction (inner-loop) and then rotated by a regular angle in k_x-k_y plane (outer-loop), ii) regular rotating SoS (REG$_{rot}$) – each new read-out is advanced by both a regular step in k_z and rotated by a regular angle in k_x-k_y, iii) a regular step, golden angle SoS (RSGA) - a regular step in k_z (inner-loop) followed by a golden angle rotation in k_x-k_y (outer-loop) (10,20) – see supporting material for full diagram - Supporting Fig. 1.

These acquisition strategies were tested on simple image space model that mimicked the main structures in the thoracic cavity (ascending and descending aorta and pulmonary arteries as cylinders;
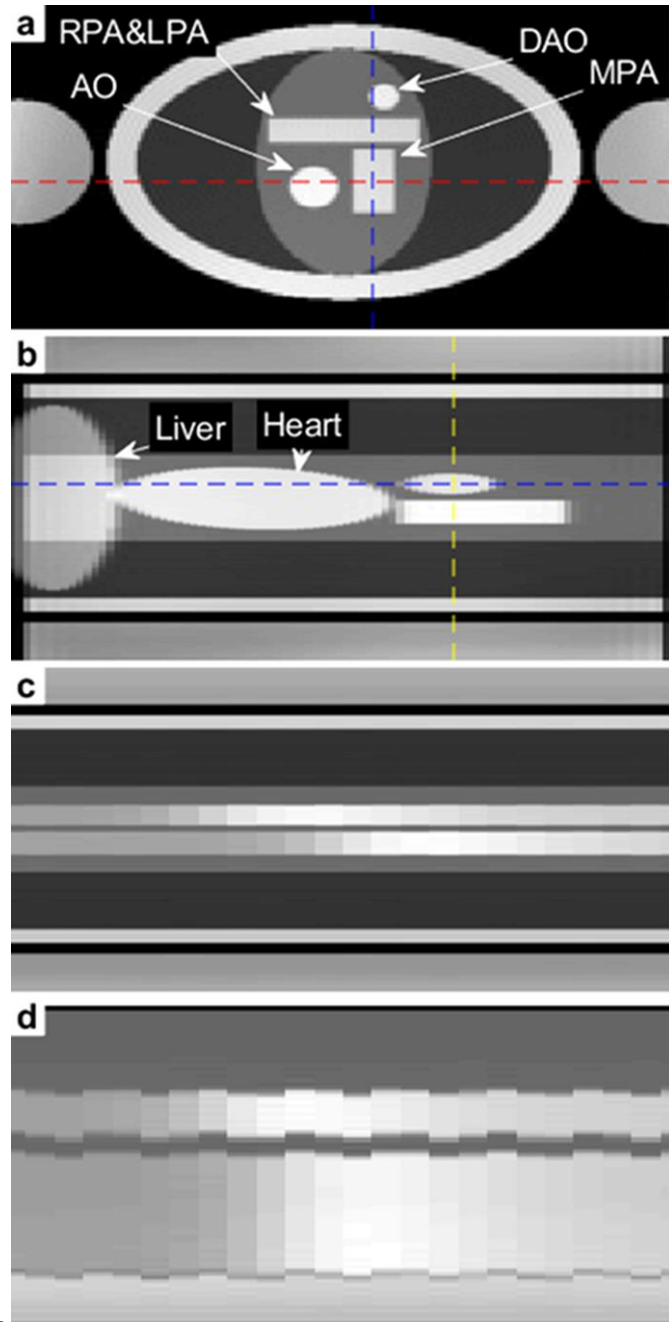
the heart and dome of liver as ellipsoids) -

Fig. 1. During the simulated cardiac cycle (72 beats/minute – the approximate average adult heart rate) the cross-sectional areas of the vessels were varied to

imitate normal arterial distension (see supporting materials - Supporting Fig. 3). While in the respiratory cycle (15 breaths/minute – the approximate average adult respiratory rate) all intrathoracic structures were periodically translated in the head foot direction (see supporting materials - Supporting Fig. 3). Two separate experiments were prepared to examine the accuracy of cardiac gated and time resolved reconstructions of the different SoS approaches against a reference standard. For the time resolved experiment, additional time varying contrast changes were also included (see supporting materials - Supporting Fig. 3).

The image volumes were generated using MATLAB (MathWorks, Inc., Natick, Massachusetts USA). To generate each spiral interleave, a model at the appropriate point in the cardiac and respiratory cycles (as well as correct contrast in the time resolved experiment) was created. The generated volume was scaled with synthetically generated coil sensitivity maps (12 coils as in the in-vivo experiment). This was then transformed into regularly sampled k-space data and gridded onto the spiral trajectory. Gaussian noise (Independent and identically distributed) was added to the generated k-space data to achieve 20 dB signal to noise ratio. For time resolved reconstructions data was reconstructed using consecutive interleaves (132 interleaves per volume = 12x undersampling). For the cardiac gated reconstructions, the model's cardiac and respiratory signals were used to perform simulated respiratory self-navigation and retrospective cardiac gating, as described above. All reconstructions were performed with multiple regularisation levels (0.01, 0.05, 0.10, 0.15, 0.20, 0.25) to ensure that the regularization was optimized for the specific sampling pattern.

Reconstructed volumes were compared against a reference standard generated using a fully sampled REG trajectory and reconstructed with the SENSE algorithm (21). Differences were separately quantified for each time point (i.e. on a per volume basis) using normalised root mean square (RMS) error.

Patient study

Ten consecutive older children and adults with congenital heart disease were enrolled into this study. Inclusion criteria were: i) clinical referral for cardiac MR imaging and ii) clinically necessary contrast enhanced MRA. Exclusion criteria were: i) general contraindications to MR, such as pregnancy or MR-incompatible implants,

ii) arrhythmia and iii) breathlessness or abnormal breathing patterns. The local research ethics committee approved the study and written consent was obtained from all subjects/guardians. The GRASS-MRA was compared to conventional breath-hold magnetic resonance angiography (BH-MRA) and SSFP cine imaging.

The conventional clinically indicated BH-MRA was performed using a 3D Cartesian spoiled gradient echo (SPGR) sequence, acquired in the sagittal orientation (FOV: 256x410x256 mm, Matrix: 160x256x160, Pixel size: 1.6x1.6x1.6 mm, TR/TE: 1.92/0.82 ms, GRAPPA factor (k_x-k_y/k_z): 2x/1x, Flip Angle: 25°). Optimal timing was ensured through the use of a 2D thick slab SPGR bolus tracking sequence. In all patients, early and late phase angiograms (~13.5 s breath-hold each) were acquired after a single injection of contrast agent, with a 15 s pause between them. The BH-MRA was performed first as this was the clinically indicated scan (mean time between BH-MRA and GRASS-MRA was 20 ± 2 minutes). A SSFP cine of the ascending aorta was planned at the level of the sino-tubular junction and was acquired with retrospective cardiac gating (FOV: 380x323 mm, Matrix: 240x204, pixel size: 1.58x1.58x8 mm, TR/TE: 2.52/1.15 ms, Flip Angle: 68°, 2xGRAPPA, ~temporal resolution 40ms) in a breath-hold.

Image Quality and Vessel Measurements in Patients study

All image data was analysed using the OsiriX open source DICOM viewing platform (Osirix 6.0, OsiriX foundation, Switzerland) [22]. Qualitative image scores of the angiographic techniques (BH-MRA and GRASS-MRA's) were rated by two observers (V.M. and K.M >10 years experience in CMR). The observers were presented with volumetric data (peak contrast for time resolved GRASS-MRA and peak systole for cardiac gated GRASS-MRA) in a multi-planar reformat viewer in a random order. Observers were blinded to the patient identity and the acquisition type. Quality was rated on a 5 point Likert scale (1 = non-diagnostic, 2 = poor, significant residual artefact and inadequate delineation of great vessels, 3 = moderate, some residual artefacts but reasonable delineation of great vessels, 4 = good, very little artefact with good great vessel visualization and 5 = excellent, no obvious artefact with ideal vessel delineation). True quantification of SNR in images acquired using sparse-parallel reconstruction is non-trivial, due to the uneven distribution of noise [23]. Therefore, we estimated SNR by dividing the signal intensity (SI) in the aorta by the standard deviation of SI in the spinal CSF (very low signal) [6]. This method only

works for angiographic techniques (BH-MRA and GRASS-MRA) and therefore this analysis was not performed on the cine SSFP data. For the time resolved GRASS-MRA reconstruction, SNR was estimated in the volume with the highest aortic contrast and for the cardiac gated GRASS-MRA reconstruction the peak systolic frame was used.

Vessel edge sharpness (ES) was calculated across the border of the sino-tubular junction of the aorta. A univariate 5th order polynomial was fitted to the normalized pixel intensities to prevent erroneous edge sharpness calculations due to noise pixels. The final ES was then calculated by measuring the maximum gradient of the fitted line. Vessel ES was evaluated for all sequences (cine SSFP, BH-MRA and GRASS-MRA) in the aorta at the level of the sino-tubular junction, in peak systole for cardiac gated data and at peak contrast for time resolved data.

Vessel diameter measurements were made in the aortic short axis at the level of the sino-tubular junction for all sequences (cine SSFP, BH-MRA and GRASS-MRA). For the time resolved reconstruction, vessel measurements were made in the volume with the highest aortic contrast. For the cardiac gated GRASS-MRA and cine SFFP data, vessel measurements were made at peak systole and end diastole.

Statistical Analysis

All statistical analysis was performed using R software (R Foundation for Statistical Computing, Vienna, Austria) and a p-value of less than 0.05 indicated a significant difference. The results are expressed as the mean ± standard deviation. For the in-silico model, RMS error differences between the four SoS approaches were assessed using one-way repeated measures analysis of variance (ANOVA). Each temporal volume was treated as a separate 'subject' and the different SoS approaches were treated as the repeated measure factor. Significant results were further investigated with post-hoc pairwise comparison using the Tukey method. In the patient study, differences between quantitative metrics of image quality and vessel size using different acquisitions were also assessed using repeated measures ANOVA. The different acquisitions were treated as the repeated measures factor and any significant results were further investigated with post-hoc pairwise comparison using the Tukey method. Qualitative image scores were compared using the Kruskal-

Wallis test. Bland-Altman and correlation analysis was performed to assess agreement of vessel measurements.

RESULTS

In Silico study

Time resolved reconstruction – The lowest RMS errors were achieved with regularisation levels set at GRASS: 0.20, RSGA: 0.10, REG: 0.15 and REG$_{rot}$: 0.15. The GRASS (0.0314 ± 0.0038) produced significantly lower ($P < 0.001$) RMS errors than the other sampling patterns - RSGA (0.0344 ± 0.0043), REG (0.0346 ± 0.0044) and REG$_{rot}$ (0.0360 ± 0.0045). There was no significant difference ($P > 0.09$) between RSGA, REG or REG$_{rot}$. These differences can be seen in
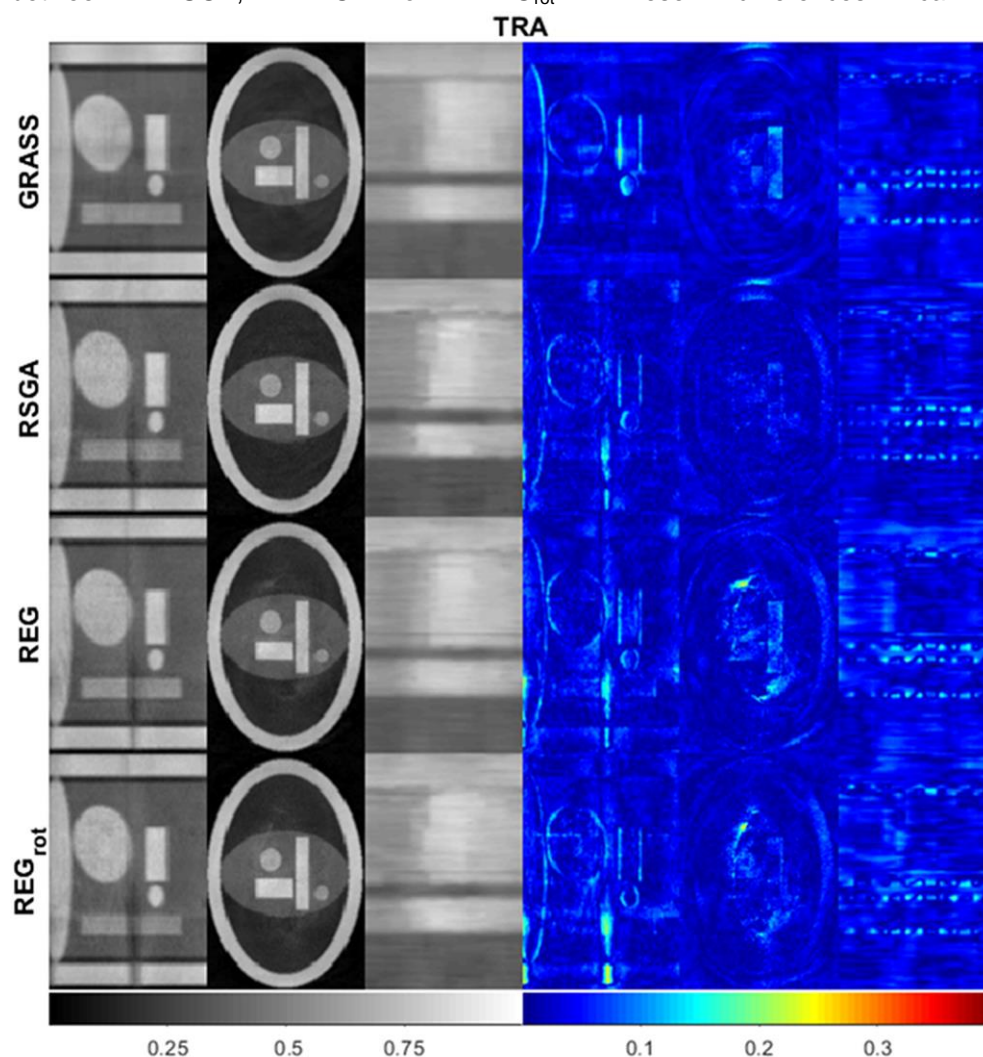
Fig. 2. It should be noted that in all of the reconstructions the respiratory motion is heavily blurred.

Cardiac gated reconstruction – The lowest RMS errors were achieved with the following regularisation parameters - GRASS: 0.15, RSGA: 0.10, REG: 0.20 and REG$_{rot}$: 0.15. The RMS error for GRASS (0.0311 ± 0.0021) was significantly lower ($P < 0.0001$) than RSGA (0.0365 ± 0.0016), REG (0.0394 ± 0.0034) and REG$_{rot}$ (0.0384 ± 0.0027). In addition, the RMS error for RSGA was significantly lower than REG and REG$_{rot}$ ($P = 0.03$). There was no significant difference in RMS error between REG and

REG~rot~. The better image quality of GRASS can be seen in
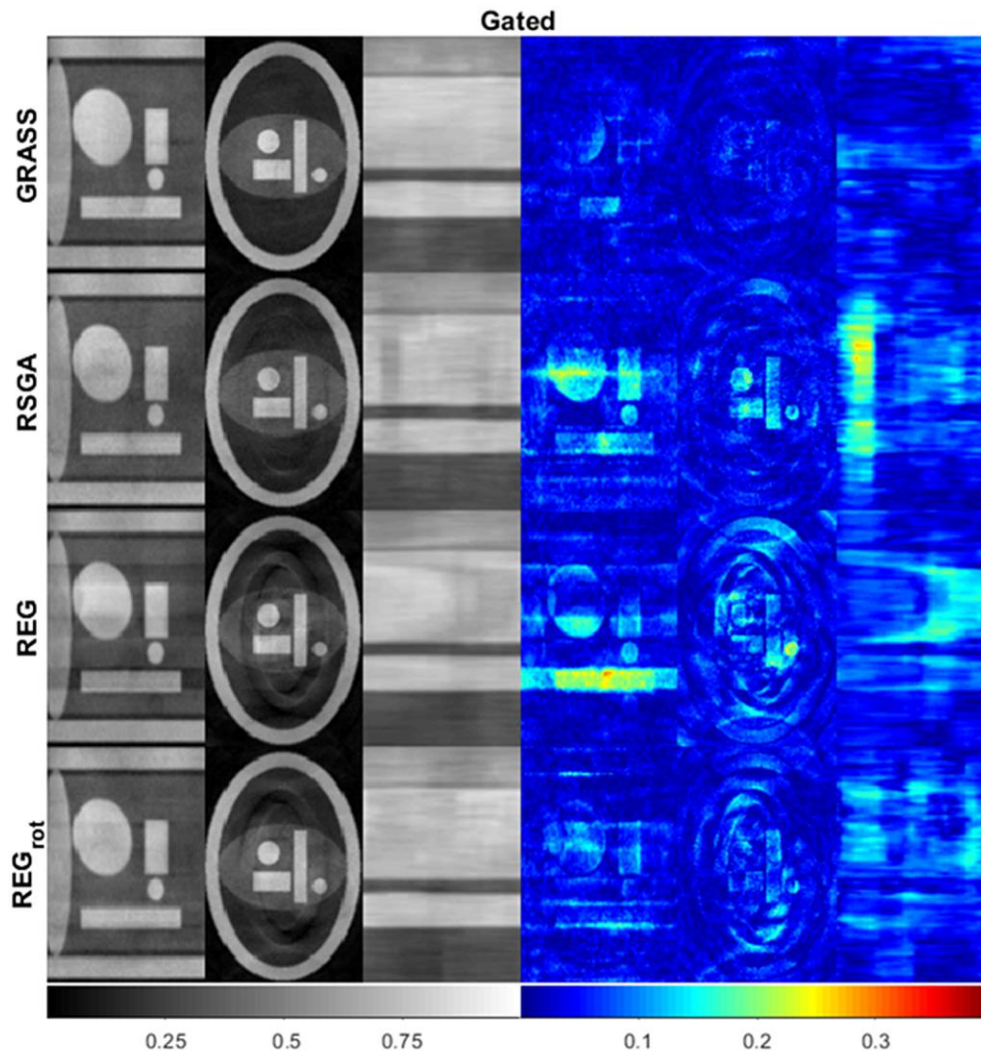
Fig. 3.

Patient study

The mean patient age was 26.9 ± 11.8 years (range: 13 to 50 years). The GRASS MRA sequence was successfully acquired and reconstructed (time resolved and cardiac gated) in all patients.

Image quality

Multi-planar reformats (MPR's) and volume renders from multiple time points of the time resolved GRASS-MRA reconstruction are shown in
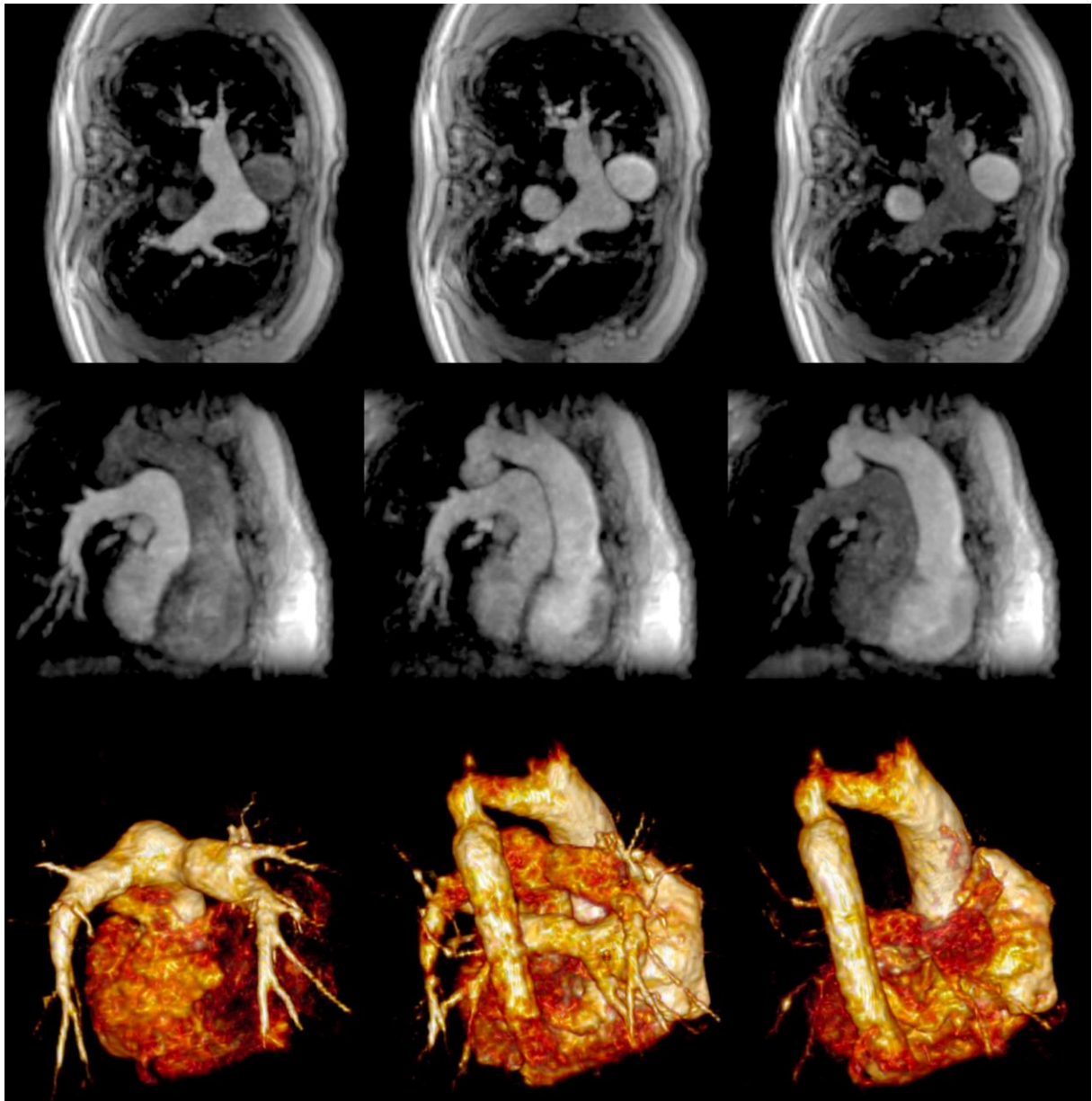
Fig. 4.
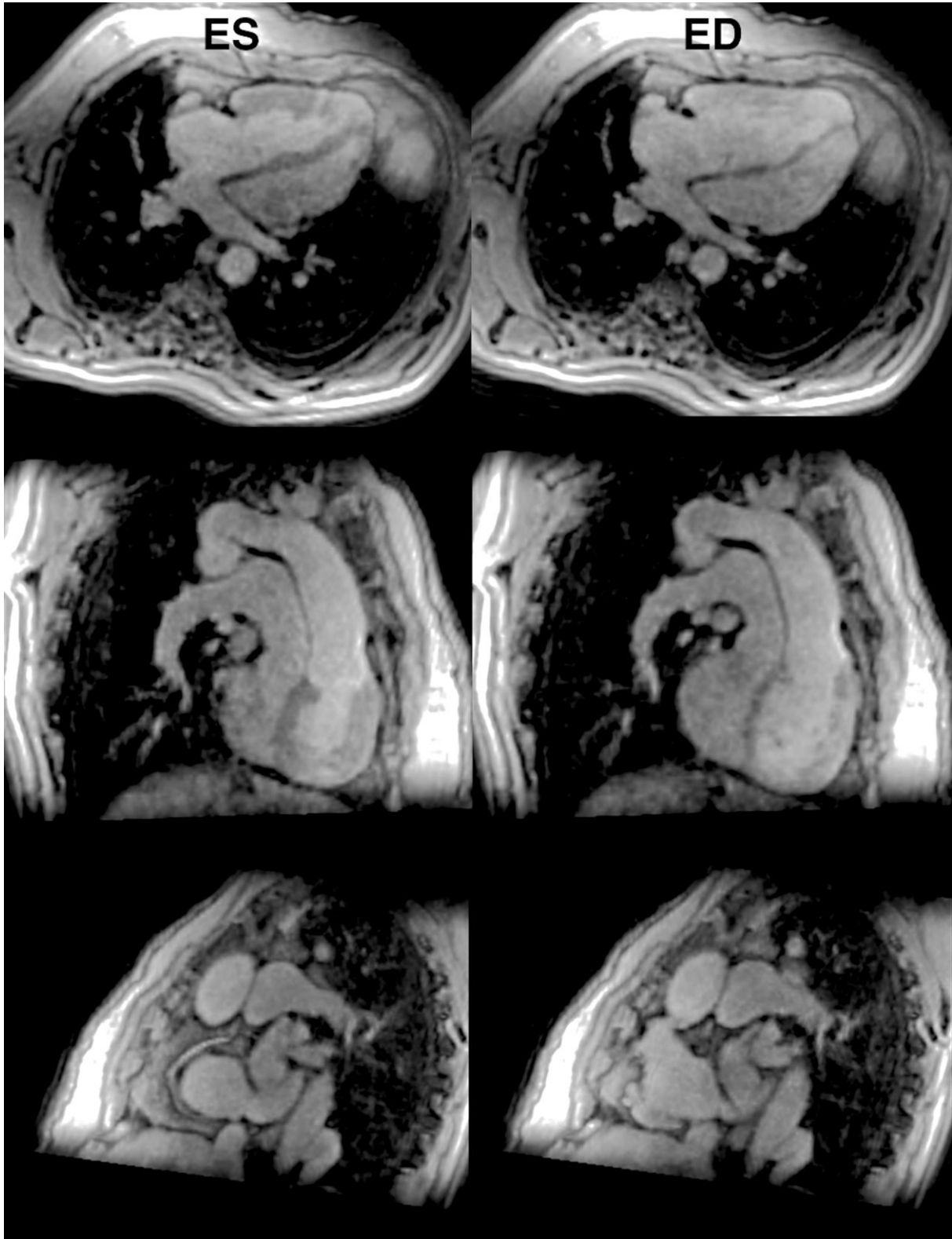
Fig. 5 shows example MPR's at end systole and diastole of the cardiac gated GRASS-MRA reconstruction. Movie clips of these two reconstructions are included in the supporting materials (Supporting Video S1-S6).

There was no significant difference ($P = 0.27$) in qualitative image scores between the BH-MRA (4.15 ± 0.6), the cardiac gated GRASS-MRA (4.35 ± 0.7) and the time resolved GRASS-MRA (3.95 ± 0.8).

The estimated SNR's for both cardiac gated (11.7 ± 3.5) and time resolved (18.8 ± 5.7) GRASS-MRA were lower ($P < 0.001$) than the BH-MRA (54.7 ± 16.8), but not different from each other ($P = 0.21$). Edge sharpness's in all the tested techniques were significantly different from each other ($P < 0.03$). The values in descending order were: cine SSFP (0.332 ± 0.058), cardiac gated GRASS-MRA (0.238 ± 0.045) time resolved GRASS-MRA (0.154 ± 0.050) and BH-MRA (0.109 ± 0.031). These differences can be seen in representative patients in
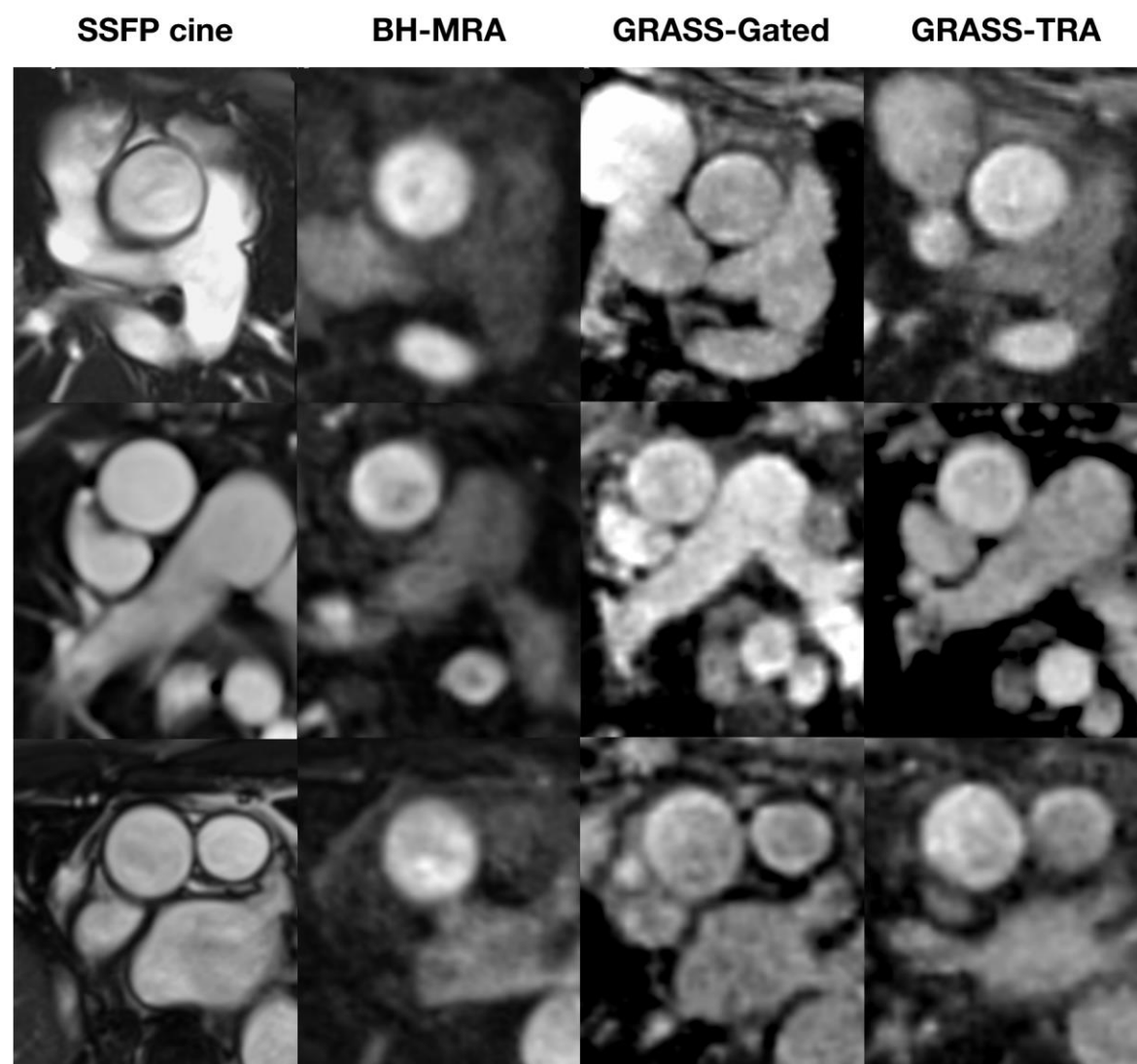
Fig. 6.

Vessel Measurements

Aortic diameter was not significantly different ($P > 0.87$) measured using BH-MRA (29.8 ± 5.6 mm), time resolved GRASS-MRA (29.9 ± 5.4 mm), diastolic cine SSFP (29.4 ± 5.8 mm), and diastolic cardiac gated GRASS-MRA (29.5 ± 5.5 mm). However, all were significantly ($P < 0.0001$) lower than aortic dimeter measured using systolic cine SSFP (32.2 ± 4.8 mm) and systolic cardiac gated GRASS-MRA (32.2 ± 5.0 mm).

There was good agreement with insignificant bias between the cardiac gated GRASS-MRA and the cine SSFP data in both systole (bias = -0.06 ± 0.87 mm, limits of agreement -1.76 to 1.64 mm) and diastole (bias = -0.10 ± 0.65 mm, limits of agreement = -1.38 to 1.18 mm). There was also good agreement between the time resolved GRASS-MRA and BH-MRA measurements (bias = -0.08 ± 0.69 mm, limits of agreement = -1.42 to 1.26 mm) as shown in
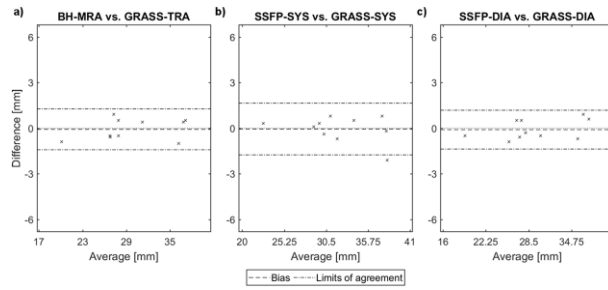
Fig. 7.

DISCUSSION

Stack of spirals is a highly efficient method of filling k-space that has previously been used for time resolved MR angiography (6). In this study, we sought to optimize this approach to enable both time resolved and cardiac gated reconstructions of the same raw data. This requires an acquisition strategy that ensures good image quality for different collections of interleaves. Golden ratio ordering is one solution and we have combined golden ratio ordering with the SoS approach. The novel aspect of our implementation is that we use golden ratio ordering in both k_x-k_y (golden angle) and k_z (golden step). The specific findings of this study were: i) The image quality of time resolved GRASS technique was comparable to a regular step, golden angle approach and superior to regular SoS approaches in an in-silico model, ii) In the cardiac gated in-silico experiment, image quality of GRASS was superior to all three alternative SoS approaches, iii) It was feasible to acquire GRASS-MRA data in patients and generate both time resolved and cardiac gated reconstructions, iv) There was good agreement in vessel measurements between the GRASS-MRA reconstructions and conventional MRI techniques.

In-silico study

The first part of this study involved comparing the GRASS acquisition with other more conventional SoS approaches. This part of the study was performed in an in-silico model as it was not feasible to acquire multiple contrast-enhanced MRA's in patients. A further benefit of the in-silico model over a more conventional static phantom study was the ability to include cardiac and respiratory motion, as well as contrast changes. For the time resolved reconstruction we demonstrated that GRASS had lower RMS errors than the other three approaches. We believe that this is because including the golden step reduces the coherency of the aliases, thus improving compressed sensing reconstruction (11,16,24). It should be noted that the compressed sensing reconstruction does results in significant blurring of respiratory motion. For angiography, this would only be clinically important if it affected measurement of vessel size. This is better assessed in-vivo as discussed in the next section. For the cardiac gated reconstructions, GRASS also had lower reconstructions errors compared to the other SoS approaches. This was presumably due to the better distribution of k-space lines when cardiac and respiratory binning is used.

However, it should be noted that substantial RMS errors were observed for all SoS approaches. For the time resolved reconstruction, this may partly be due to respiratory motion effects and temporal blurring. For the cardiac gated reconstruction, these errors were probably due to a combination of high acceleration factors and uneven gaps in k-space. Nevertheless, GRASS sampling did produce lower RMS error for both time resolved and cardiac gated reconstructions. The clinical significance of these differences in RMS error is difficult to quantify, but residual artefacts could potentially make detection of subtle abnormalities more difficult.

Patient study

We demonstrated the feasibility of reconstructing both time resolved and cardiac gated angiograms from the same GRASS raw data in patients with congenital heart disease. This is a group of patients in whom the ability to evaluate the passage of contrast and make accurate vessel measurements throughout the cardiac cycle is important. Other benefits of the GRASS technique are that it can be performed during free-breathing and it is relatively motion insensitive. Both of these may be useful when imaging children.

In terms of image quality, both time resolved and cardiac gated GRASS-MRA had lower SNR than BH-MRA, even though the clinically indicated BH-MRA was acquired at higher resolution. This is to be expected due the much greater acceleration of GRASS-MRA compared to BH-MRA (~12x vs. 2x). Both time resolved and cardiac gated GRASS-MRA did have better edge sharpness than BH-MRA. This is interesting as the BH-MRA was acquired at higher resolution. The reason for this difference is probably the reduced cardiac motion artefact associated with GRASS-MRA (particularly with the cardiac gated GRASS-MRA). From a clinical point of view better vessel sharpness may aid accurate delineation the vessel border when making vessel diameter measurements. However, lower SNR might make border delineation more difficult and therefore an important aspect of this study was to compare diameters measured using the different techniques. We demonstrated good agreement between time resolved GRASS-MRA and BH-MRA. We also showed good agreement between systolic and diastolic diameters measured from the cardiac gated GRASS-MRA and cine SSFP. These data suggest that irrespective of the lower SNR and better edge sharpness, measurements made using GRASS-MRA are

comparable to conventional techniques. Another issue is the temporal blurring caused by the CS reconstruction. For instance, in the in-silico study we demonstrated significant blurring of respiratory motion in time resolved GRASS model. However, in the patient study this did not seem to affect the accuracy of time-resolved GRASS-MRA vessel measurements. In cardiac gated GRASS-MRA temporal blurring could result in reduced systolic/diastolic differentiation. Yet we found there was good agreement for systolic and diastolic vessels measurements between cardiac gated GRASS-MRA and cine SSFP. This suggests that CS related temporal blurring is not clinically significant in the cardiac gated angiographic setting.

The main advantage of GRASS-MRA is the ability to perform both time resolved and cardiac gated reconstructions from the same raw data acquired during free breathing. Time resolved angiography is useful in congenital heart disease as it provides information about the passage of contrast that can be used to identify certain congenital lesions. Cardiac gated MRA on the other hand enables assessment of diameters at different points in the cardiac cycle, which can be useful in certain groups of patients (i.e. congenital patients undergoing endovascular interventions or patients with aortopathy). In addition, the ability to perform angiography during free breathing is particularly useful in children as they often find breath-holding for conventional MRA difficult. We believe that these benefits offset the increased overall scan and reconstruction times associated with the GRASS technique.

Limitations

In this study, we decided to use the SoS approach due it's efficiency in filling k-space and previous use in congenital heart disease (6). However, there are some problems with spiral imaging, which have not been addressed in this study. These include susceptibility to off-resonances and trajectory errors, which can result in artefacts. However, no obvious blurring was observed and the read-out times were kept short (~9 ms) to reduce the potential trajectory errors. Alternative approaches such as radial stack of stars may be less prone to trajectory errors and off-resonances, although they are less efficient at filling k-space (10). Thus, in future studies a direct comparison of radial and spiral techniques is warranted. It should be noted that golden step, golden angle ordering is equally applicable to stack of stars and should provide similar benefits to those seen in this study. The final limitation were long

reconstruction times even using a GPU reconstruction (~25 min). Thus, more work is required in developing faster algorithmic approaches (i.e. alternating direction method of multipliers). Newer algorithmic approaches (such as blind CS (25) and data driven models (26)) might also be important in improving image quality, particularly when using higher acceleration factors.

Conclusion

We have described a stack of spirals approach that utilizes both golden step and golden angle ordering. It has been shown that this approach enables cardiac gated and time resolved reconstruction of the same data. This technique may be particularly beneficial in the assessment of congenital heart disease, enabling fast simple evaluation of the vasculature.

Acknowledgments

REFERENCES

1.   Geva T, Greil GF, Marshall AC, Landzberg M, Powell AJ. Gadolinium-enhanced 3-dimensional magnetic resonance angiography of pulmonary blood supply in patients with complex pulmonary stenosis or atresia: comparison with x-ray angiography. Circulation 2002;106(4):473-478.

2.   Greil GF, Powell AJ, Gildein HP, Geva T. Gadolinium-enhanced three-dimensional magnetic resonance angiography of pulmonary and systemic venous anomalies. J Am Coll Cardiol 2002;39(2):335-341.

3.   Prasad SK, Soukias N, Hornung T, et al. Role of magnetic resonance angiography in the diagnosis of major aortopulmonary collateral arteries and partial anomalous pulmonary venous drainage. Circulation 2004;109(2):207-214.

4.   Ferrari VA, Scott CH, Holland GA, Axel L, Sutton MS. Ultrafast three-dimensional contrast-enhanced magnetic resonance angiography and imaging in the diagnosis of partial anomalous pulmonary venous drainage. J Am Coll Cardiol 2001;37(4):1120-1128.

5.   Valsangiacomo ER, Levasseur S, McCrindle BW, MacDonald C, Smallhorn JF, Yoo SJ. Contrast-enhanced MR angiography of pulmonary venous abnormalities in children. Pediatr Radiol 2003;33(2):92-98.

6.   Steeden JA, Pandya B, Tann O, Muthurangu V. Free breathing contrast-enhanced time-resolved magnetic resonance angiography in pediatric and adult congenital heart disease. J Cardiovasc Magn Reson 2015;17:38.

7.   Groves EM, Bireley W, Dill K, Carroll TJ, Carr JC. Quantitative analysis of ECG-gated high-resolution contrast-enhanced MR angiography of the thoracic aorta. AJR Am J Roentgenol 2007;188(2):522-528.

8.   Winkelmann S, Schaeffter T, Koehler T, Eggers H, Doessel O. An optimal radial profile order based on the Golden Ratio for time-resolved MRI. IEEE Trans Med Imaging 2007;26(1):68-76.

9.   Steeden JA, Knight DS, Bali S, Atkinson D, Taylor AM, Muthurangu V. Self-navigated tissue phase mapping using a golden-angle spiral acquisition-proof of concept in patients with pulmonary hypertension. Magn Reson Med 2014;71(1):145-155.

10. Feng L, Grimm R, Block KT, et al. Golden-angle radial sparse parallel MRI: combination of compressed sensing, parallel imaging, and golden-angle radial sampling for fast and flexible dynamic volumetric MRI. Magn Reson Med 2014;72(3):707-717.

11. Tolouee A, Alirezaie J, Babyn P. Compressed sensing reconstruction of cardiac cine MRI using golden angle spiral trajectories. J Magn Reson 2015;260:10-19.

12. Coppo S, Piccini D, Bonanno G, et al. Free-running 4D whole-heart self-navigated golden angle MRI: Initial results. Magn Reson Med 2015;74(5):1306-1316.

13. Cheng JY, Zhang T, Ruangwattanapaisarn N, et al. Free-breathing pediatric MRI with nonrigid motion correction and acceleration. J Magn Reson Imaging 2015;42(2):407-420.

14. Irarrazabal P, Nishimura DG. Fast three dimensional magnetic resonance imaging. Magn Reson Med 1995;33(5):656-662.

15. Deng W, Zahneisen B, Stenger VA. Rotated stack-of-spirals partial acquisition for rapid volumetric parallel MRI. Magn Reson Med 2016;76(1):127-135.

16. Lyu J, Spincemaille P, Wang Y, Zhou Y, Ren F, Ying L. Highly accelerated 3D dynamic contrast enhanced MRI from sparse spiral sampling using integrated partial separability model and JSENSE. Proc of SPIE Vol, 2014.

17. Hargreaves BA. Variable-Density Spiral Design Functions. Volume 2016.

18. Lenz GW, Haacke EM, White RD. Retrospective cardiac gating: a review of technical aspects and future directions. Magn Reson Imaging 1989;7(5):445-455.

19. Adluru G, Awate SP, Tasdizen T, Whitaker RT, Dibella EV. Temporally constrained reconstruction of dynamic cardiac perfusion MRI. Magn Reson Med 2007;57(6):1027-1036.

20. Liu J, Spincemaille P, Codella NC, Nguyen TD, Prince MR, Wang Y. Respiratory and cardiac self-gated free-breathing cardiac CINE imaging with multiecho 3D hybrid radial SSFP acquisition. Magn Reson Med 2010;63(5):1230-1237.

21. Pruessmann KP, Weiger M, Bornert P, Boesiger P. Advances in sensitivity encoding with arbitrary k-space trajectories. Magn Reson Med 2001;46(4):638-651.

22.   Rosset A, Spadola L, Ratib O. OsiriX: An Open-Source Software for Navigating in Multidimensional DICOM Images. J Digit Imagin 2004;17(3):205-216.

23.   Dietrich O, Raya JG, Reeder SB, Reiser MF, Schoenberg SO. Measurement of signal-to-noise ratios in MR images: influence of multichannel coils, parallel imaging, and reconstruction filters. J Magn Reson Imaging 2007;26(2):375-385.

24.   Feng L, Axel L, Chandarana H, Block KT, Sodickson DK, Otazo R. XD-GRASP: Golden-angle radial MRI with reconstruction of extra motion-state dimensions using compressed sensing. Magn Reson Med 2016;75(2):775-788.

25.   Lingala SG, Jacob M. Blind compressive sensing dynamic MRI. IEEE Trans Med Imaging 2013;32(6):1132-1145.

26.   Velikina JV, Samsonov AA. Reconstruction of dynamic image series from undersampled MRI data using data-driven model consistency condition (MOCCO). Magn Reson Med 2015;74(5):1279-1290.
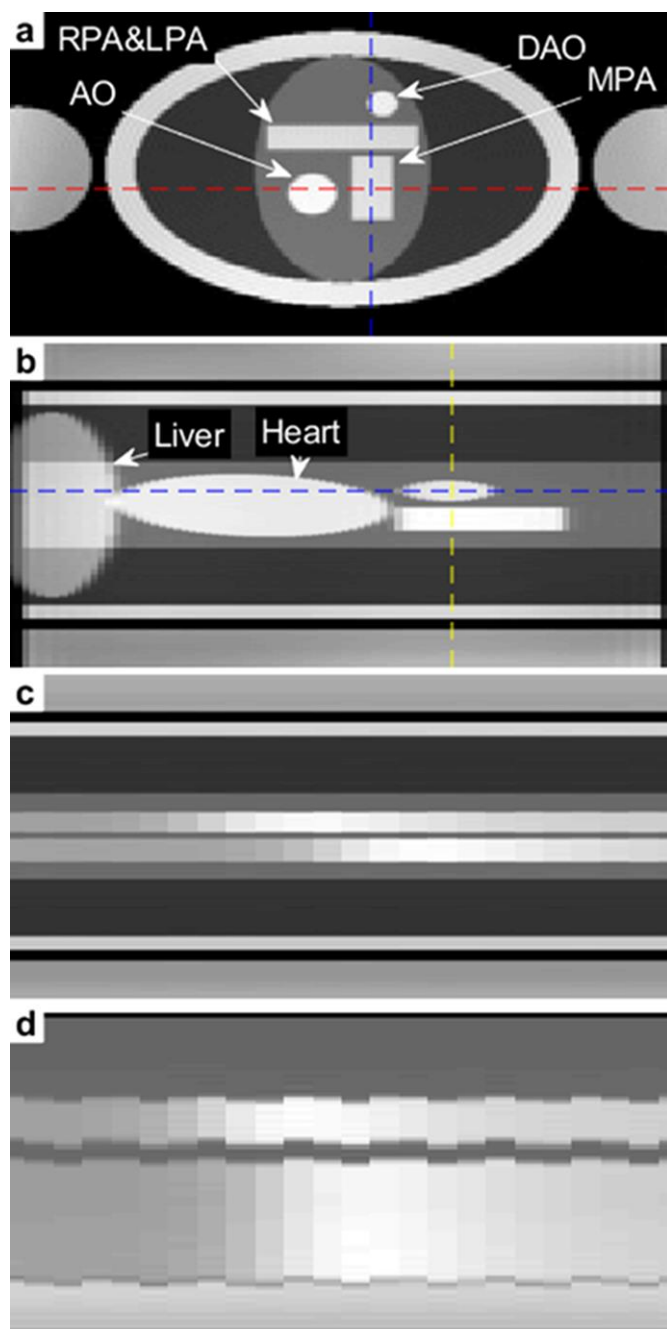
Fig. 1. The figure presents the basic structure of the in-silico model. From the top: a) transversal cut across model (marked by the yellow line on Fig 2b) showing the chest wall modelled as cylinder with two adjacent cylinders representing arms. Inside the body cylinder there are four cylinders representing ascending (AO) and descending aorta (DAO), left and right pulmonary arteries (LPA&RPA), and middle pulmonary artery (MPA). These were surrounded by a low signal mediastinal cylinder. b) a coronal cut (marked by the red line on Fig 2a) showing two ellipsoids representing liver and heart in addition to the vascular structures. c) a time-lapse of a 1D cut (a red-yellow dash-lines intersection) showing the contrast and changes in the vessel structures. d) a time-lapse of 1D cut (a red-blue dash-lines intersection) showing contrast changes, as well as respiratory motion.
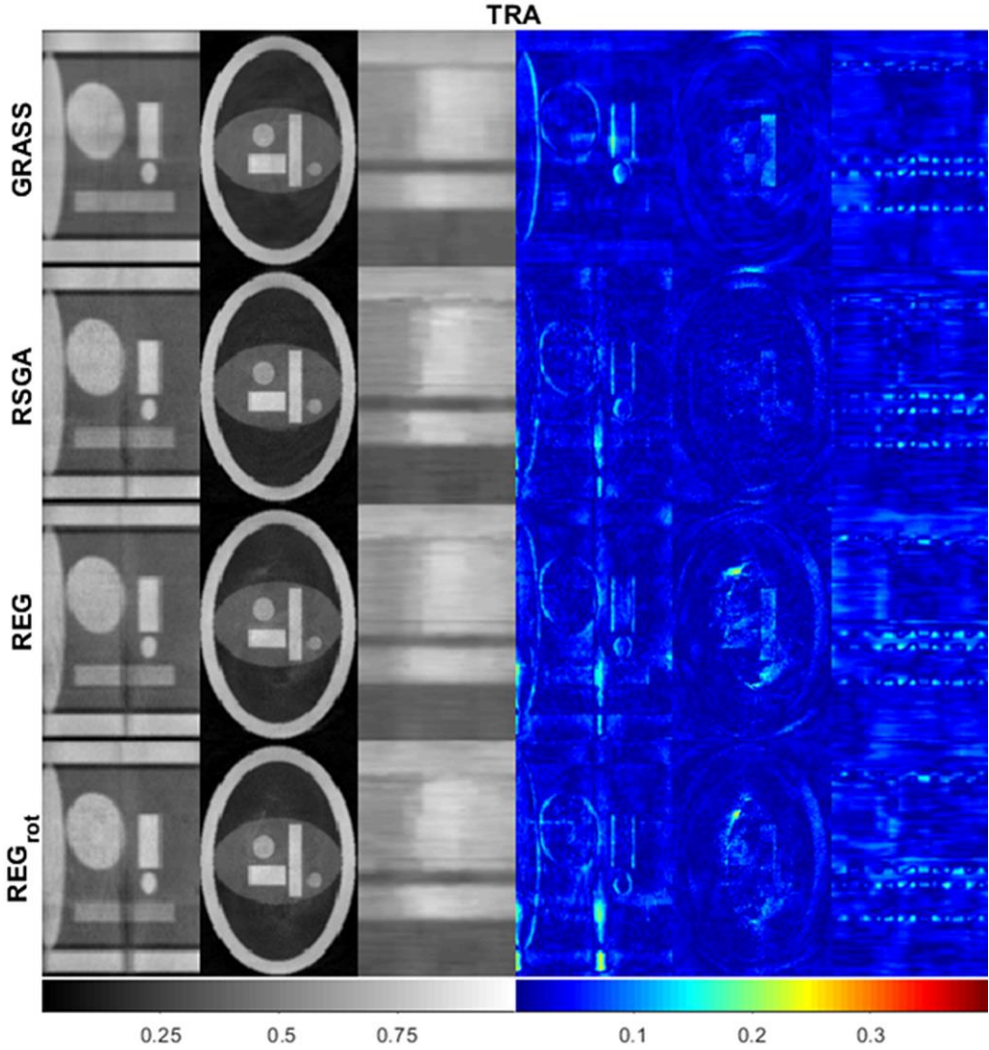
Fig. 2. Results for the time resolved reconstructions in the in-silico model. Sagittal and transversal cross sections of a single volume with contrast in both the aorta and pulmonary artery, and temporal
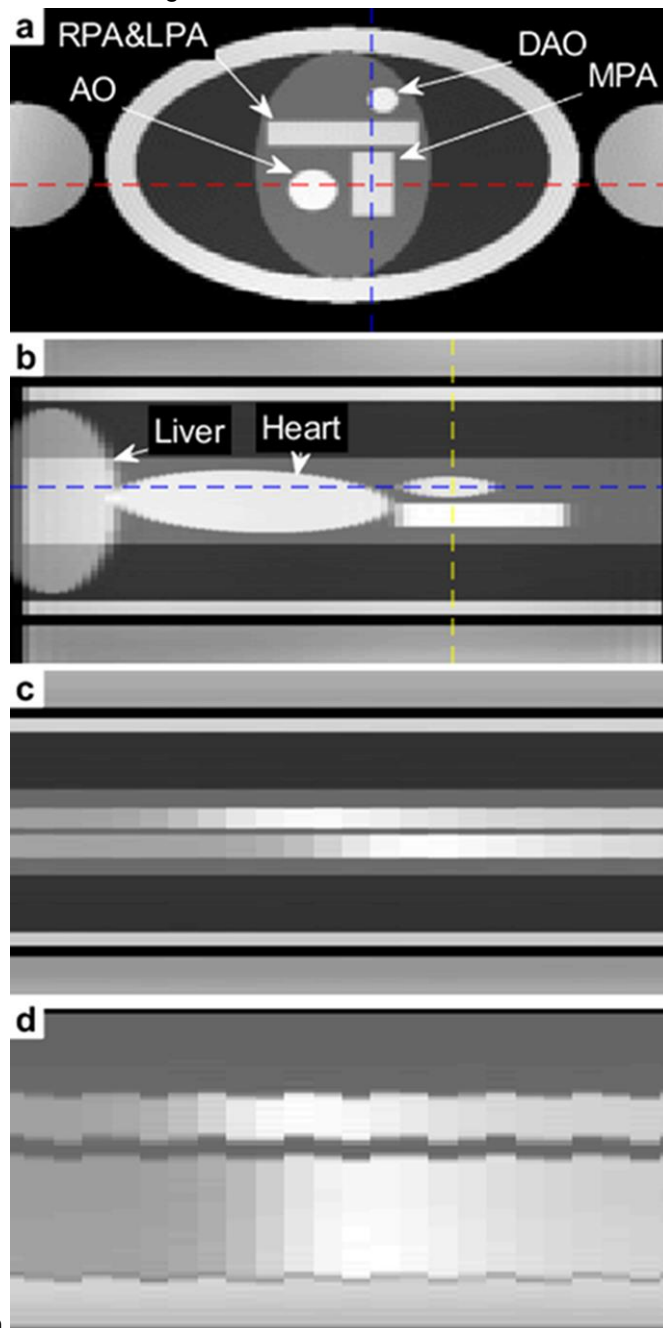
cut (as in Fig. 1d) are presented. The magnitude data was normalised and is presented on the left with the magnitude difference images on the right as compared to the fully sampled reference. The results for individual trajectories are presented in rows in the following order: Golden RAtio Stack of Spirals (GRASS), Regular Step, Golden Angle stack of spirals (RSGA), Regular stack of spirals (REG) and Rotated regular stack of spirals (REG$_{rot}$).
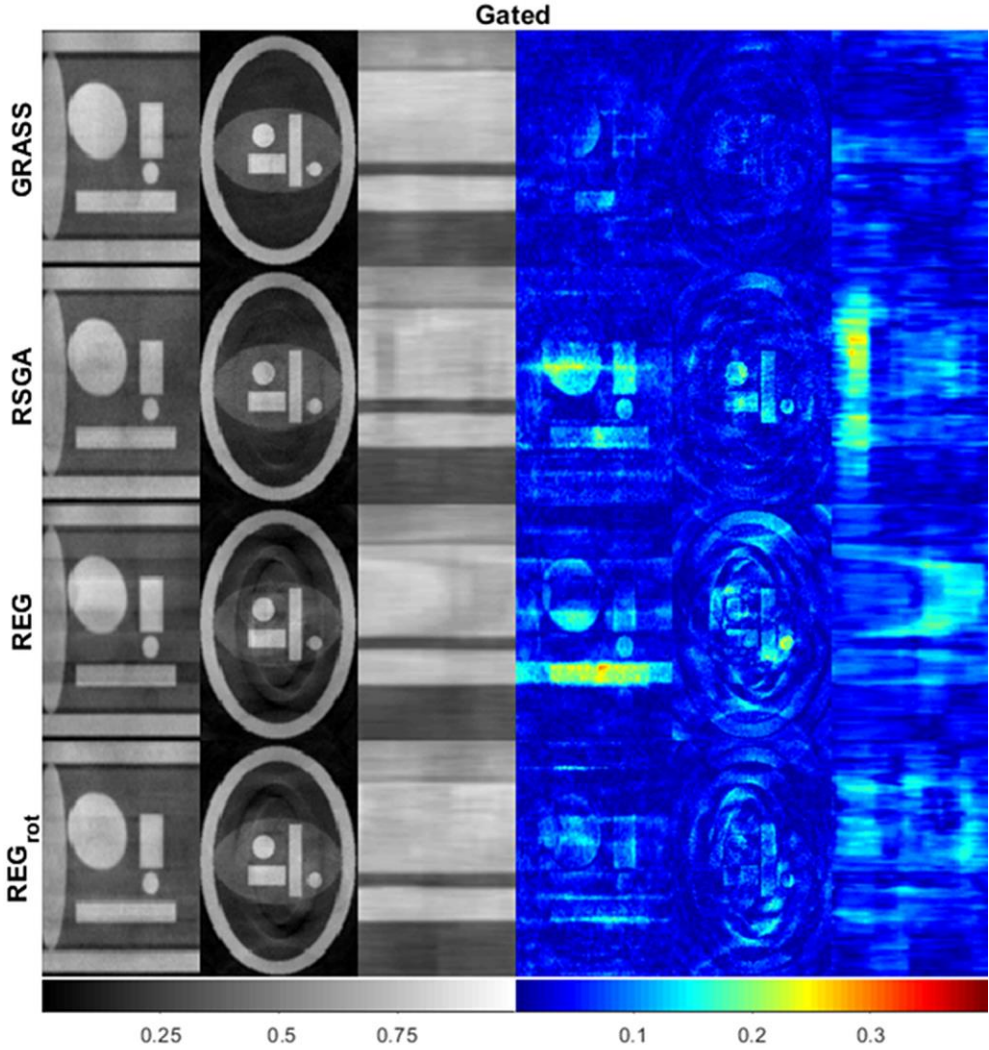
Gated

Fig. 3. Results for the retrospectively gated reconstructions in the in-silico model. Sagittal and transversal cross sections of a single systolic volume, and temporal cut (as in
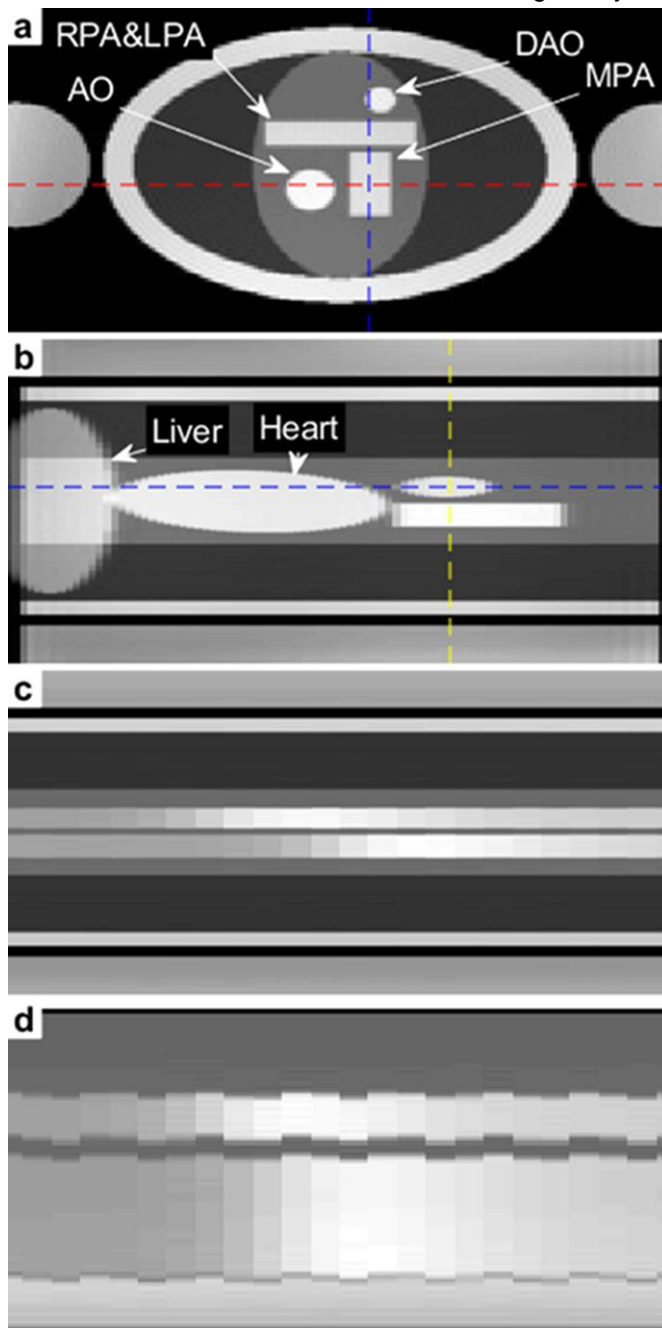
Fig. 1d) are presented. The magnitude data was normalised and is presented on the left with the magnitude difference images on the right as compared to the fully sampled reference. The results for individual trajectories are presented in rows in the following order: Golden RAtio Stack of Spirals (GRASS), Regular Step, Golden Angle stack of spirals (RSGA), Regular stack of spirals (REG) and Rotated regular stack of spirals (REG$_{rot}$).
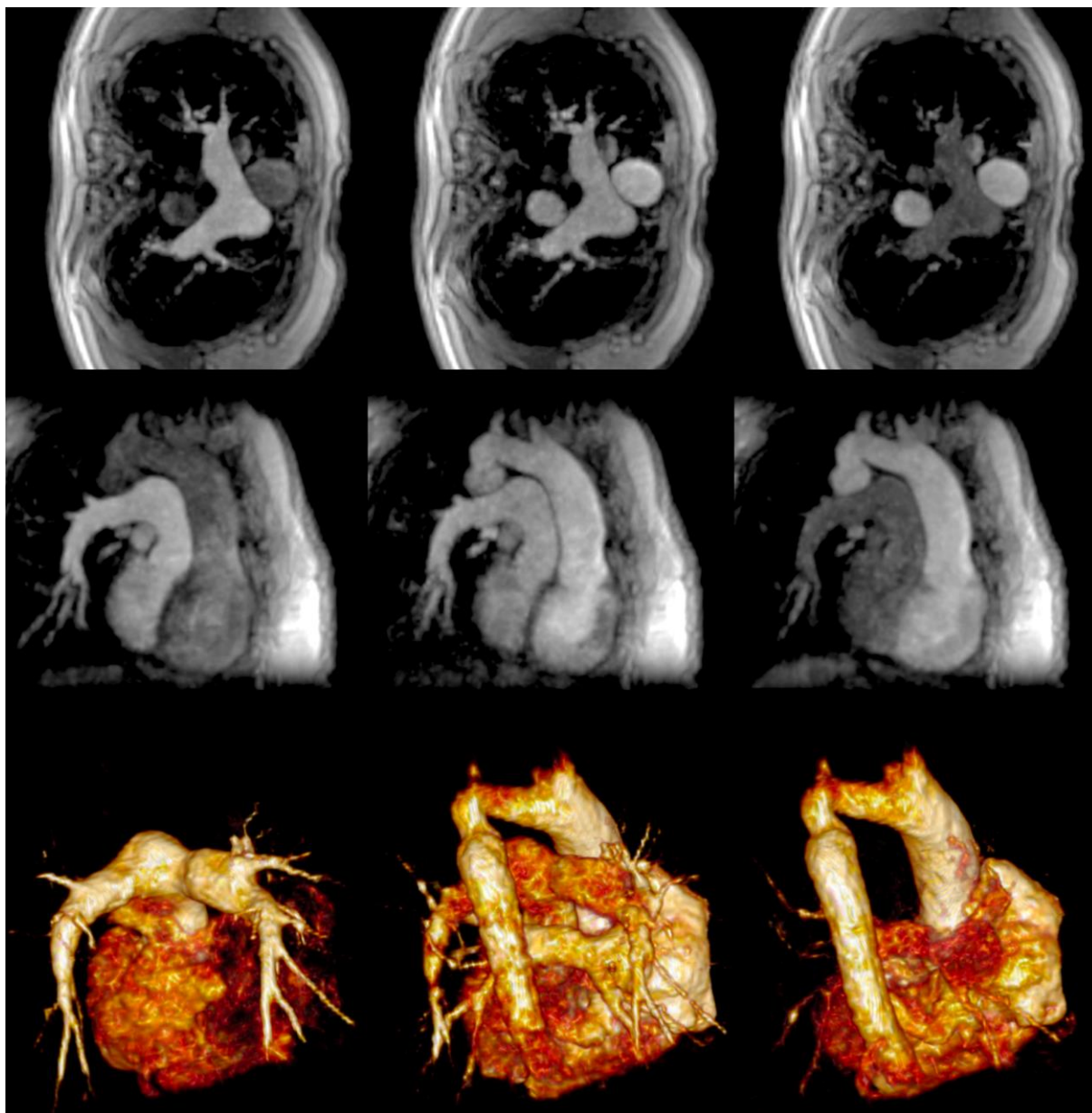
Fig. 4. Time Resolved reconstruction of the GRASS-MRA in a patient with transposition of the great arteries treated with an Atrial switch. The top row shows axial oblique multi-planar reformats (MPR's) through the pulmonary arteries. The middle row shows sagittal oblique MPR's through the great vessels with the aorta anterior. The bottom row shows volume renders viewed from the back. The columns represent different time points after contrast administration.
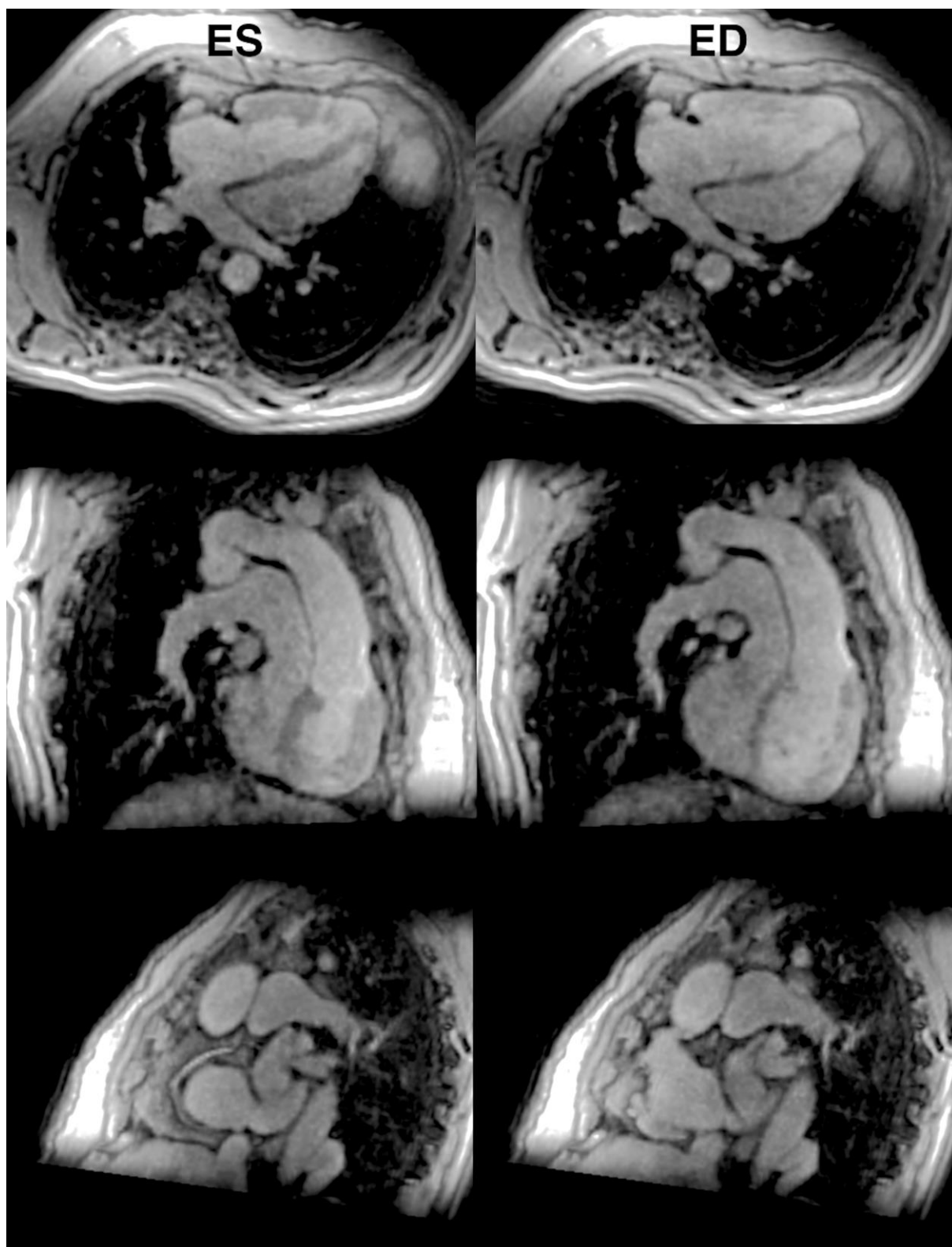
Fig. 5. Cardiac gated reconstruction of the GRASS-MRA in a patient with transposition of the great arteries treated with an Atrial switch. The top row shows axial oblique multi-planar reformats (MPR's) through the pulmonary venous baffle and 4-chamber of the heart. The middle row shows sagittal oblique MPR's through the great vessels with the aorta anterior. The bottom row shows sagittal oblique MPR's through the right coronary. The left column is at end systole (ES) and the right column is at end diastole (ED).
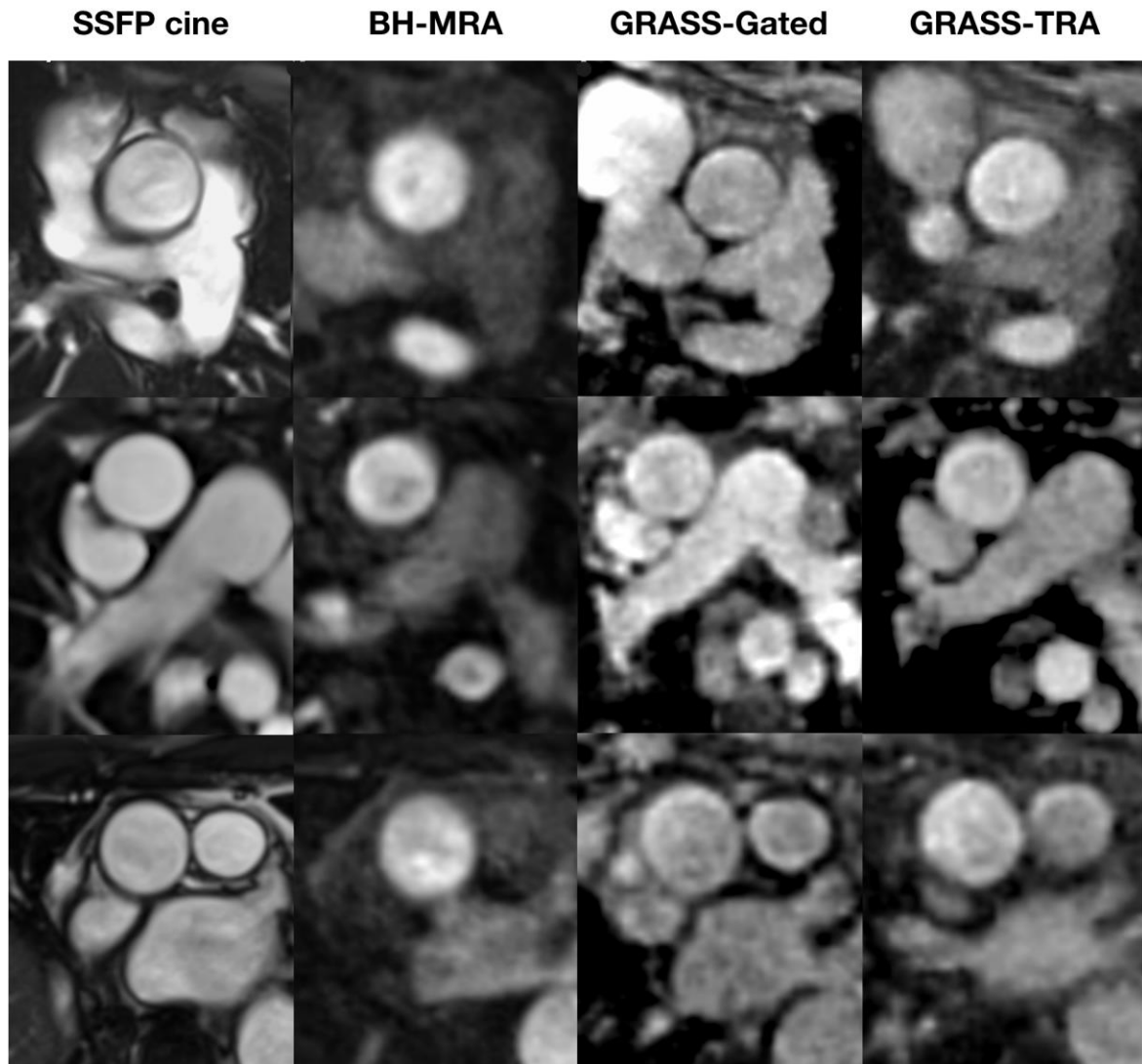
Fig. 6. Examples of images quality of the different techniques in a slice planned through the ascending aorta in three patients. First column - Steady State Free Precession cine (SSFP cine), second column - Conventional breath-hold contrast enhanced angiogram (BH-MRA), third column - Cardiac Gated GRASS angiogram (GRASS-Gated) and fourth column - Time resolved GRASS angiogram (GRASS-TRA).
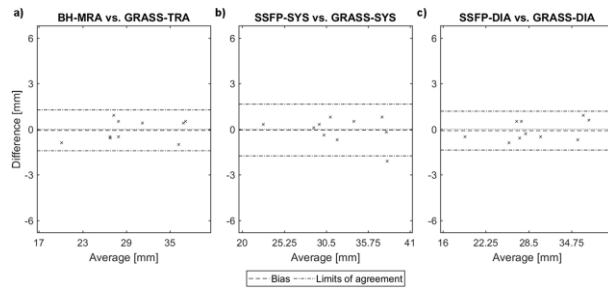
Fig. 7. Bland Altman plots comparing vessel measurements between different techniques.
From the left: a) breath-hold MR angiography (BH-MRA) vs. time resolved GRASS-MRA (GRASS-TRA); b) the systolic frame in the Cine SSFP (SSFP-SYS) vs the systolic frame of cardiac gated GRASS-MRA (GRASS-SYS); c) the diastolic frame in the Cine SSFP (SSFP-DIA) vs the diastolic frame of cardiac gated GRASS-MRA (GRASS-DIA).

SUPPORTING MATERIALS
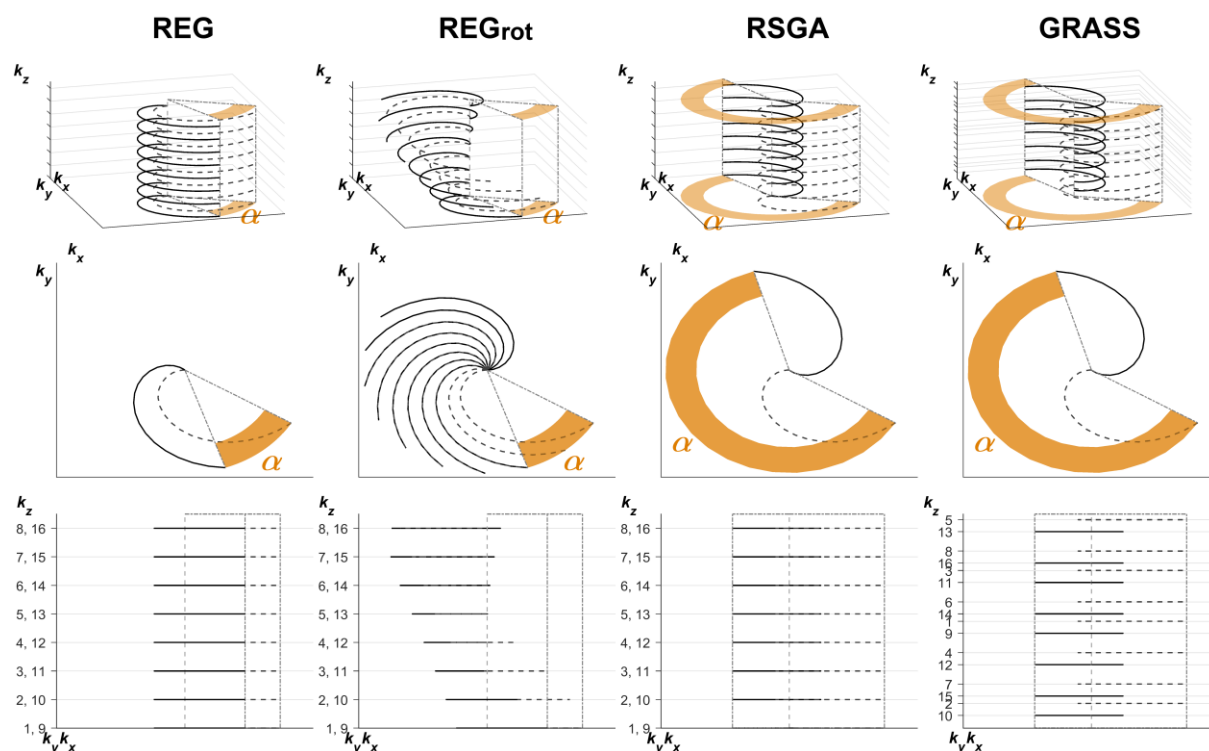
Supporting Fig. 1 Simplified representation of the acquisition strategy of the golden ratio stack of spirals (GRASS) scheme, the regular angle and step (REG) scheme and its rotating variant (REG$_{rot}$) and the regular step, golden angle (RSGA) scheme. The top row shows a subset of read-outs acquired in 3D k-space (k_x, k_y, k_z). The middle row shows the read-outs positions in k_x, k_y being rotated by different angular rotations (α) during the outer-loop operation depending on the acquisition. The bottom row shows the read-outs progression in k_z. The line styles gather read-outs assigned to different outer loop iterations (solid line – current, dashed line – previous). The read-out indices are printed in the bottom row showing their distribution in k_z direction.
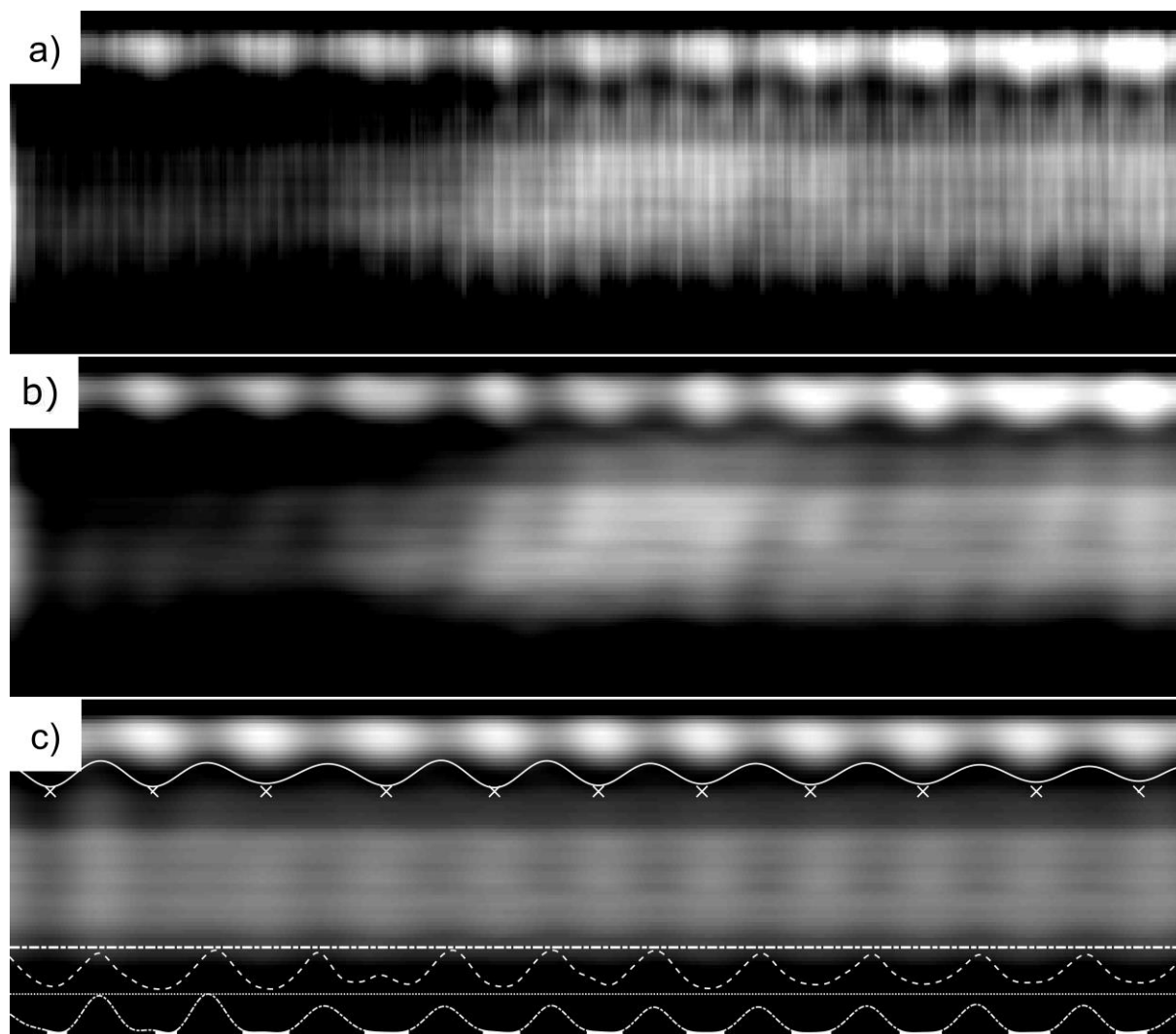
Supporting Fig. 2 Schematic of the processing for creation of the respiration navigator signal.

The raw signal derived from Fourier transformation of the central axis of k-space is shown in (a) with cardiac, respiratory and contrast variations exhibited. The cardiac signal was removed using an adaptive low-pass filter to generate an intermediate result (b). The intermediate result still exhibited slowly varying blood contrast changes and this can be removed using a band-pass filter concentrated around the highest peak in the assumed respiration frequency range. This produced the final result (c), which was used to generate the navigator signal. Firstly the centre-of-mass (represented with the solid white line) was calculated, which was used to select the peak-expiratory positions (marked with the white x). These were used to generate the averaged reference projection. The correlation coefficient of all the lines against the reference (the '-.' white line at the bottom) was used to select 30% of the data (marked with the white area under the correlation line). For comparison the simultaneously acquired bellows data was overlaid above the correlation plot (the '--' white line).
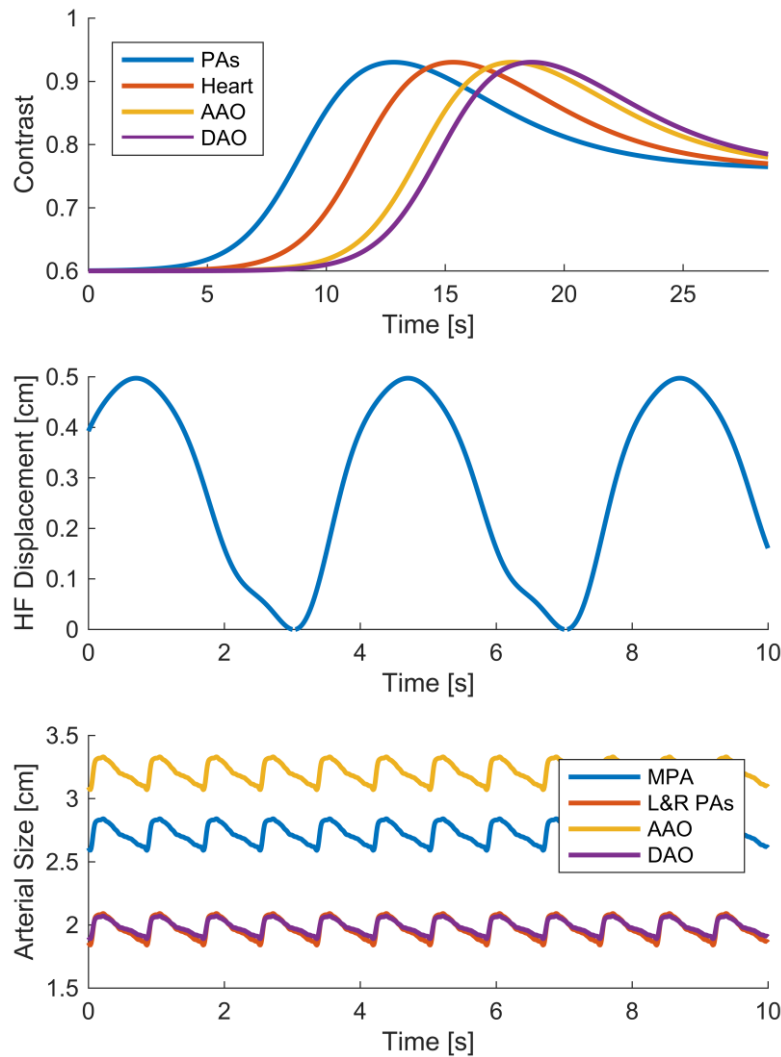
Supporting Fig. 3 In-silico phantom temporal changes functions.
(a) Contrast change over time for the heart, ascending (AAO) and descending aorta (DAO) and pulmonary arteries (PAs). Each of these curves is modelled as the sum of two generalised logistic functions, one of them being an ascending sigmoid and the other being a descending sigmoid. They are all identical except for their time delays. The y axis represents the actual contrast in the in-silico model, which is in the range [0, 1]. (b) Displacement in the head-foot direction of thoracic structures due to breathing. This curve was obtained from a human subject by processing a free-breathing 2D real-time cine sequence in which diaphragmatic motion was apparent. The centre of mass of a head-foot (HF) line through the diaphragm's upper bound was calculated for all time points, and the resulting signal was low-pass filtered to remove noise. A standard breathing cycle was then taken and replicated at the desired breathing frequency. (c) Arterial size changes. A Cartesian high-resolution retrospective cine SSFP was used as a reference to simulate vessel diameter changes in the in-silico model.

Supporting Video S1 Axial oblique multi-planar reformats through the pulmonary arteries for Time Resolved reconstruction of the GRASS-MRA in a patient with transposition of the great arteries treated with an Atrial switch.

Supporting Video S2 Sagittal oblique multi-planar reformats through the great vessels with the aorta anterior for Time Resolved reconstruction of the GRASS-MRA in a patient with transposition of the great arteries treated with an Atrial switch.

Supporting Video S3 Volume renders viewed from the back for Time Resolved reconstruction of the GRASS-MRA in a patient with transposition of the great arteries treated with an Atrial switch.

Supporting Video S4 Axial oblique multi-planar reformats through the pulmonary venous baffle and 4-chamber of the heart for Cardiac gated reconstruction of the GRASS-MRA in a patient with transposition of the great arteries treated with an Atrial switch.

Supporting Video S5 Sagittal oblique multi-planar reformats through the great vessels with the aorta anterior for Cardiac gated reconstruction of the GRASS-MRA in a patient with transposition of the great arteries treated with an Atrial switch.

Supporting Video S6 Sagittal oblique multi-planar reformats through the right coronary for Cardiac gated reconstruction of the GRASS-MRA in a patient with transposition of the great arteries treated with an Atrial switch.